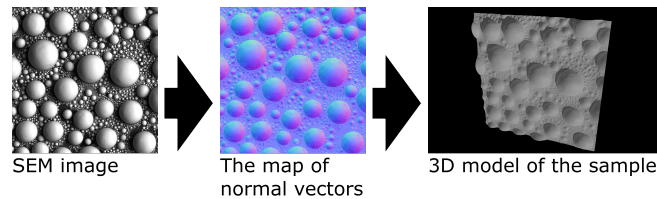


Photometric Stereo Processing for Microscopy

Samuel Repka



Abstract

This paper proposed a method of 3D reconstruction of scanning electron microscope (SEM) specimen. The aim is to explore the possibilities of topography reconstruction of microscopic samples, as well as to attempt to solve the task using tools already available on conventional scanning electron microscopes. The proposed solution uses images from a four-segment backscattered electrons detector as an input to the photometric stereo algorithm. This algorithm exploits the fact, that the brightness of the image point is dependent on the inclination of the sample surface. Reflectance maps are used to estimate the inclination in each pixel, creating a map of normal vectors. The map is then used for topography reconstruction. A novel technique for reflectance map estimation is proposed. This method is applied to tin samples to remove the sample's atomic number effects. The fact that all data are acquired simultaneously allows for fast reconstruction. Usage of already available and widespread tools eliminate a need for specialized equipment such as Atomic Force Microscopes.

Keywords: Photometric stereo — Scanning electron microscope — 4-segment BSE detector

Supplementary Material: [Repository with the code](#)

*xrepka07@stud.fit.vutbr.cz, Faculty of Information Technology, Brno University of Technology

1. Introduction

The knowledge of surface topography and 3D measurements is often needed. For example, in the semiconductor industry, spatial features' details can help to design electronic circuits or to find errors in the designs. Even though the capabilities of the scanning electron microscope include the acquisition of many kinds of data, 3D surface measurement is usually not one of them.

Multiple approaches to 3D surface measurement exist. The approaches range from specialized equipment such as Atomic Force Microscope (AFM) [1] through special procedures like FIB-SEM (FIB - Focused Ion Beam) tomography [2] to pure software solutions such as photogrammetry [3]. Each of them comes with its own share of strengths and weaknesses.

In this paper, a photometric stereo method is examined and implemented.

Photometric stereo has been a research subject for over 40 years [4], but implementation in the SEM environment did not gain widespread usage. This is because of the complex calibration of calculation parameters and the influence of effects like shadowing and noisiness. This work proposes a new method of obtaining reflectance maps, which are then used to estimate the map of normals of the sample. The map of normals is used to reconstruct the surface topography. The proposed solution does not require any specialized equipment on top of a Scanning Electron Microscope (SEM) and 4-segment backscattered electrons detector, the both commonly available on SEM systems.

Accurate reflectance maps are necessary for the

precise topography reconstruction. The intensity and the angular distribution of the backscattered electrons (BSE) depend on the sample's atomic number, the inclination of the surface, and the energy of electrons [5]. On top of that, the distance between detector and sample is variable. This causes the acquisition of backscattered electrons with a different solid angle and elevation angle of the detector (see section 4). The internal setting of the detector also influences the resulting image. This work focuses on tin samples with given offset and gain to remove a few variables from the solution.

2. Backscattered electrons detector

Many designs of semiconductor detectors exist, one of which is the 4-segment detector. It consists of four separate detectors, symmetrically placed around the incident beam as seen in Figure 1. Each segment captures backscattered electrons from different spatial locations, and the signal from each segment can be represented as an image. The differences in positions of the segments cause the specimen to "be seen" as if under different lighting conditions in the resulting images (Figure 2). The acquisition of all four images is simultaneous, meaning that only a single scan is required to acquire data in all four segments. These properties make the detector ideal for the application of photometric stereo.

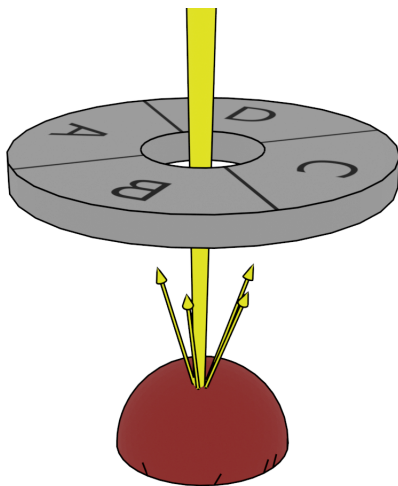


Figure 1. Schematic of the BSE detector. Yellow line in the middle is the electron beam shining on the sample (red sphere). Some electrons become backscattered ("reflected") from the sample.

3. 3D reconstruction algorithm overview

The basis of the algorithm is the estimation of the reflectance maps. The reflectance map is defined as individual brightness values assigned to points in the

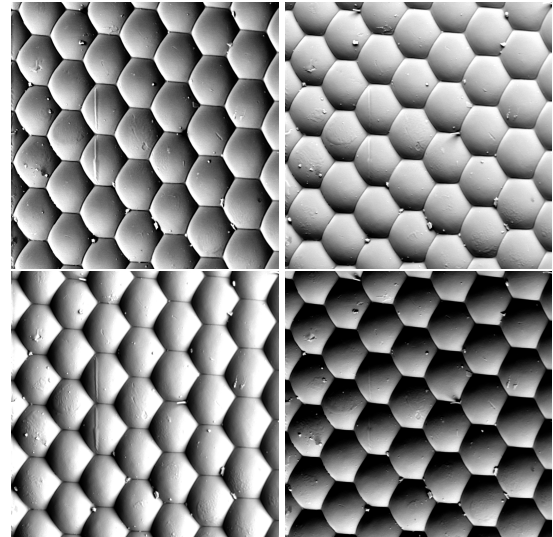


Figure 2. Four images of the same sample (eye of the fly) acquired simultaneously; each image is from a different segment of the detector. Each cell is approximately $20 \mu\text{m}$.

gradient space [4]. The gradient space is first-order partial derivatives of the surface inclination with respect to the x and y axes. However, because the possible inclination of the sample surface in SEM is $(-90^\circ, 90^\circ)$, derivatives of inclination near the edge of the spectrum would approach infinity. This imposes the problem of the representation of reflectance maps in the software. As a solution, the reflectance map is represented in the discrete "spherical" space, which has a range $(-90^\circ, 90^\circ)$, and the normal vector $[0,0,1]$ is directly in the centre. It can be easily imagined as a top-down view of the illuminated sphere (Figure 4).

This way, the reflectance map can be stored in the simple 2-dimensional matrix, where a unit normal vector represents the inclination of the surface as follows: Assuming normalized image with $[0,0]$ directly in the middle and borders in range $\langle -1, 1 \rangle$, n_x and n_y are the same as coordinates in the image. n_z can be calculated as

$$n_z = -\sqrt{1 - n_x^2 - n_y^2} \quad (1)$$

, where the subscript of n represents respective component of the vector.

The image is internally approximated via the Lamé curves (Superellipses) in order to speed up processing and save resources, as described in section 5.

The reflectance map is unique for each segment, and in the ideal case, because of the symmetrical distribution of BSE detector segments, it would be the same but rotated by 90 degrees. Reflectance maps are then used to estimate surface normal in each pixel of the image, and the created map of normal vectors is used to reconstruct the 3D model. See Figure 3.

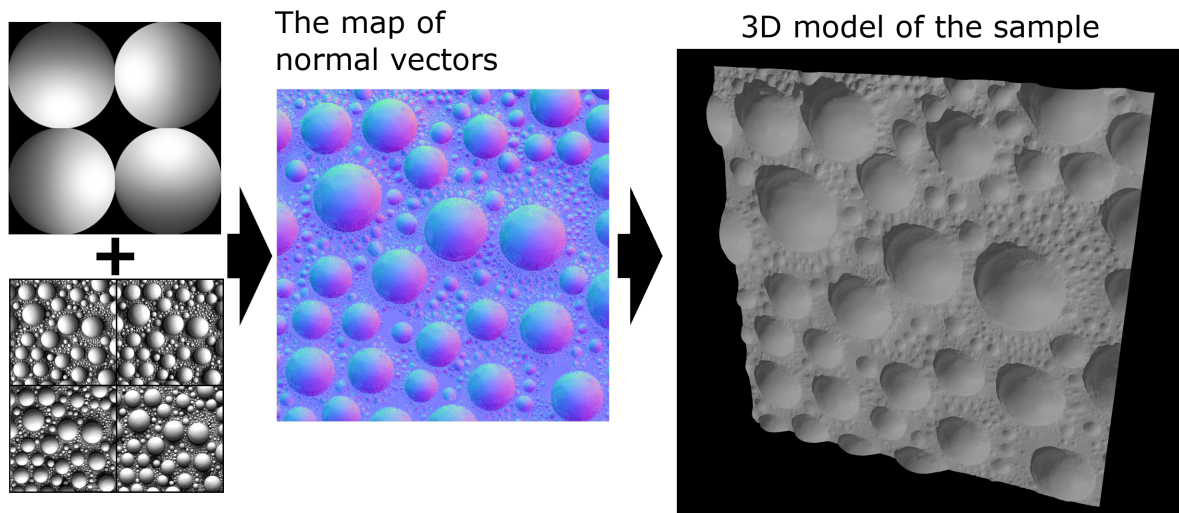


Figure 3. The overview of the algorithm steps. First, the reflectance maps are generated. Then the image of normal vectors is estimated, and the surface topography is reconstructed.

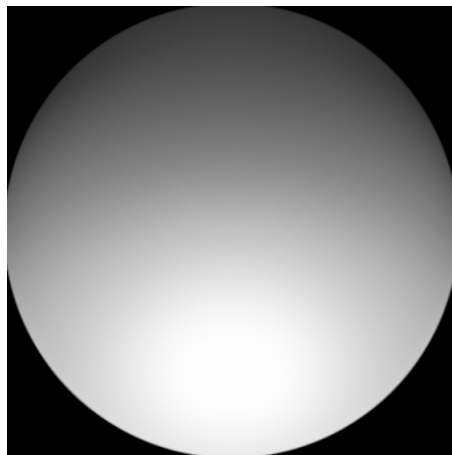


Figure 4. Reflectance map in "spherical" space.

However, using the normal map to reconstruct surface topography imposes a problem of cumulative error. The straightforward method would be an integration of the normals over the whole image. But because of the noise in the image of normal vectors, every iteration adds a more significant error the further from the starting point surface patch is.

Several methods have been employed to minimize the integration error. Most often, a method uses a least-squares approach. In this work, a grid method as described in the literature [6] is used. In the beginning, a quadrangular facet for each of the normals is created. The next phase of the algorithm is iterative and consists of two significant steps called local shaping and global blending. In local shaping, each facet is projected onto a plane defined by normal in the point. Global blending attempts to modify a mesh surface in a way that satisfies the positions of vertices in all of the facets and is not discontinuous. The error of such deformation is calculated by means of least squares. In this work, the algorithm was modified to

allow for greater deformation of facets with normals of greater inclination. This modification was done because tests have shown that measurement accuracy of normal angle drops with greater inclinations.

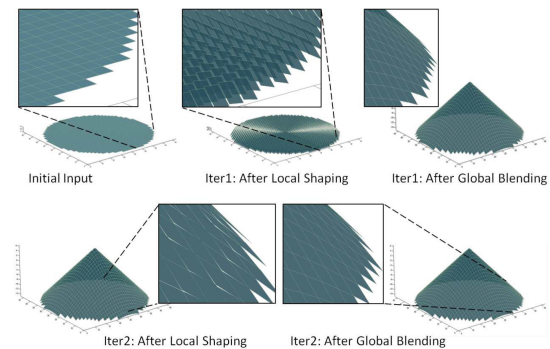


Figure 5. Visualisation of local shaping and global blending. [6]

4. Calibration of the system

The output of the BSE detector depends on several variables, which can be divided into two categories.

Properties influencing the output of backscattered electrons

- **Inclination of the surface (relative to the electron beam)** - The amount of backscattered electrons increases heavily with greater sample surface inclinations. For example, for a flat aluminium specimen with the incident beam at 15 keV with the surface normal parallel to the electron beam (angle is 0°), approximately 13% of incident electrons turn to backscattered electrons. At 85° degrees, 70% of incident electrons become backscattered electrons. At 0° , Lambert's cosine law can represent the angular dis-

tribution of backscattering. However, at bigger inclinations, the specular component becomes much more prominent [7]. See Figure 6.

- **Atomic number** - The atomic number of the specimen material significantly affects the backscattered electrons quantity and the angular distribution. With increasing atomic number, the number of backscattered electrons increases as well [5]. The angular distribution is also affected [7]. See Figure 6. This work focuses only on tin specimens, allowing for omitting this variable from the solution.
- **The energy of the incident beam** - Larger energies cause an increase in the number of backscattered electrons. The angular distribution is affected as larger energy changes the diffuse and specular component ratio of the resulting emittance. [7]. See Figure 6.
- **The beam current** - The current influences number of backscattered electrons but does not change the ratio of backscattered electrons. Thus, the image looks brighter for greater currents because of more detected backscattered electrons.

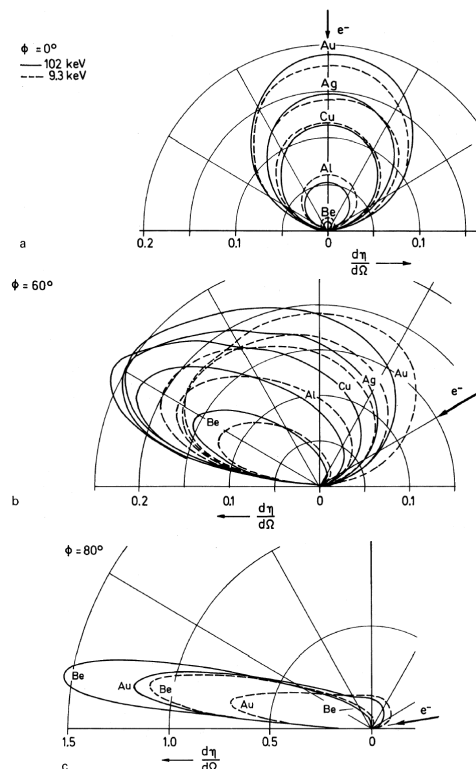


Figure 6. Illustration of polar diagrams for different tilt angles, materials and energies [7].

Properties influencing detection rates

- **Solid angle** - An important property of the detector is the solid angle Ω . It can be used to estimate an overall geometric efficiency [5]. Figure

7 shows that even though the detector D_2 has a much more extensive collection area, the solid angle is similar to that of the D_1 because of the distance from the sample.

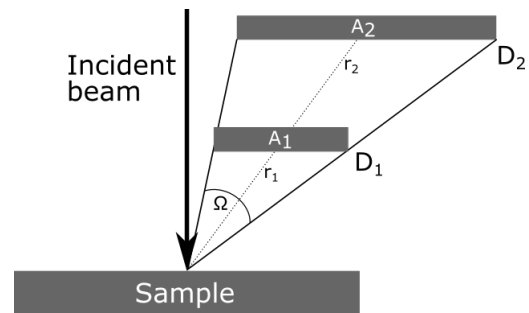


Figure 7. Solid angle - Despite detector D_2 being much larger than detector D_1 , the solid angle Ω is the same due to the D_1 being closer to the sample.

- **Distance between the detector and the sample** - SEMs are often designed to have a 4-segment BSE detector directly under the objective lens at a fixed distance. The stage with the sample, however, can move up and down. Because of the constant collection area of the detector, this means that the solid angle Ω is variable.
- **Offset and gain of the detector** - Variations in the number of collected BSE are countered by variable detector parameters that improve the output signal. These parameters are changed depending on the sample and the scanning conditions. The gain alters the contrast of the resulting signal and can be translated into a multiplication operation on the raw output of the detector. Offset, on the other hand, affects the brightness of the signal. It is a constant value added to the raw output of the detector. In this work, because of non-trivial dependencies of these parameters on the environment, constant values of the offset and gain were used.

Some of these variables can be dealt with relatively easily. The solid angle of the detector is known and constant. However, variable working distance and the energy of the incident beam influence the resulting image in a way that is difficult to calculate. Because of these effects, combined with the hardly-predictable nature of the angular distribution of backscattered electrons, an empirical novel approach was chosen.

A large dataset of tin balls was acquired. Because spheres contain every surface inclination, they are feasible for approximating reflectance maps. This dataset contains images taken at different working distances and electron energies. Subsequently, pixels with a given value were filtered for each possible value (0-

255). See Figure 8. The mask with filtered pixels would provide sufficient information to estimate the normal. However, the accuracy would be restricted by the resolution of the normal map. Moreover, these masks would need to be processed thousands of times while calculating a normal image, which is not efficient in terms of processing time and space. As a solution, an approximation of the masks with superellipses is proposed. For this application, a superellipse can be defined with five parameters. The superellipse was fitted to the masks of the dataset. The parameters for each value of (0-255) were then approximated using a spline with a set of points, allowing for dynamic generation of superellipse parameters. The points of the spline were further approximated to estimate superellipse parameters depending on the properties like the beam energy and the working distance. An example of superellipse approximation can be seen in Figure 9.

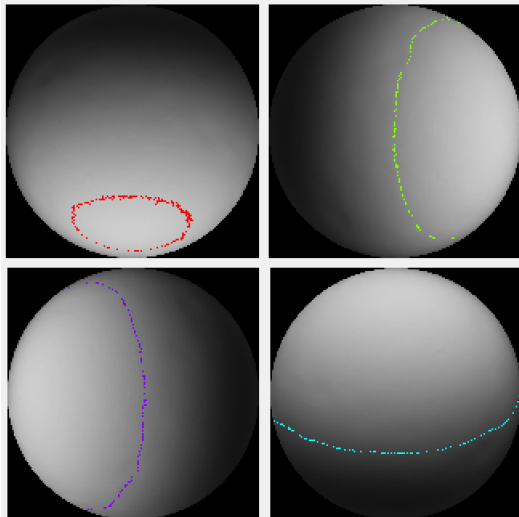


Figure 8. Reflectance map with highlighted pixels with the same intensity.

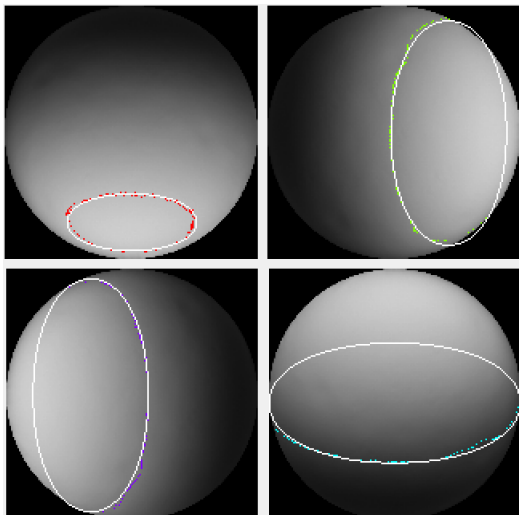


Figure 9. Colored pixel overlaid with superellipses.

5. Calculation of image normals

The algorithm used in this work is a variation of the algorithm described in the literature [4]. In this form it is used to estimate the normal vector at certain point. During the reconstruction it is iterated over the whole image.

1. One value is extracted from the same place on each image.
2. A superellipse is determined for each value, according to current microscope settings.
3. The points of interest are calculated for each superellipse pair. The points of interest are intersections of the resulting shapes or averages of the closest points in case of no intersection. In the case of multiple intersections, a point closest to the average of all points is chosen.
4. Chosen points are averaged, creating a point representing estimated normal.

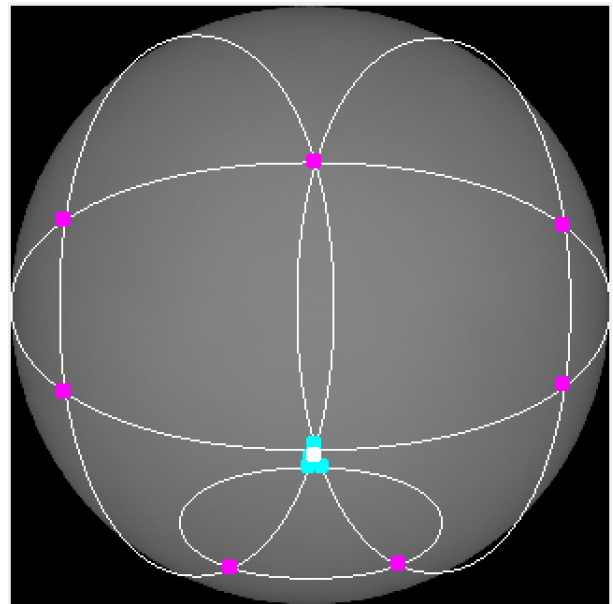


Figure 10. Overlaid masks from all maps. Magenta points are points of interest that were not chosen, whereas cyan points were chosen. The white point represents estimated normal.

6. Results

Here are some examples of the proposed solution. Even though not everything is made out of tin, the algorithm still provides a reasonable guess of the 3D model.

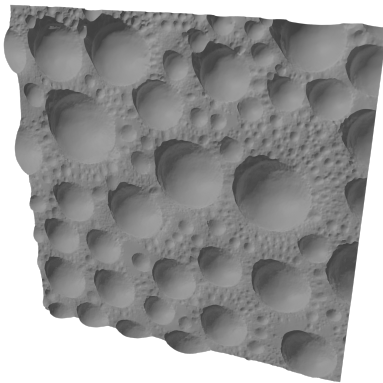
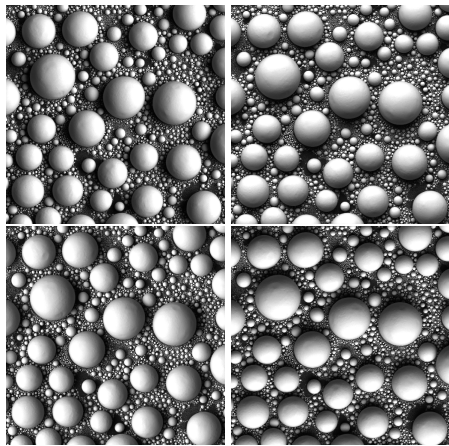


Figure 11. Input images - tin spheres.

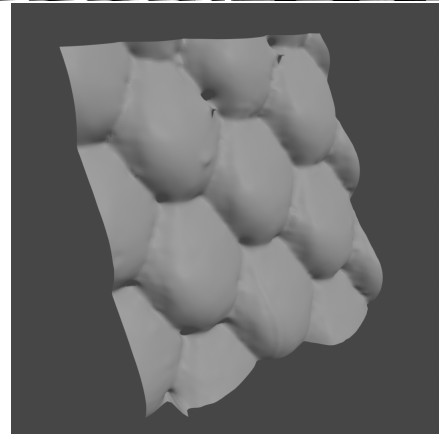
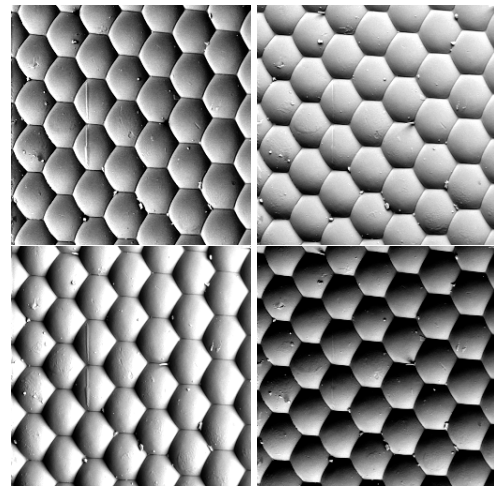


Figure 13. Input images - an eye of the fly.

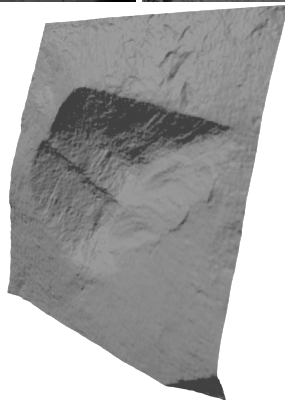
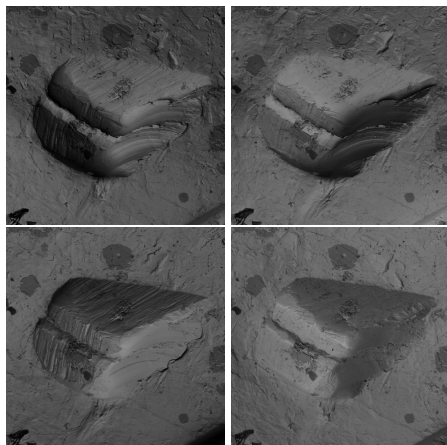


Figure 12. Input images - a ridge in the indium wire.

7. Conclusions

A new method of estimating reflectance maps was introduced. A sketch of a system for topography reconstruction of tin samples was presented. It was shown that empirical estimation of reflectance maps is a viable option when some reasonable assumptions are taken. However, this method is restricted to the available microscope-detector configuration on which it was developed. Usage of the different detector will require recalibration of the base reflectance maps.

Future research could broaden this solution to more materials. With a dataset containing enough materials, it would be possible to extrapolate knowledge on other materials based on atomic numbers. Shadowing artefacts are not taken into account. Even though photometric stereo is an excellent tool for estimation, more work is needed to ensure topography reconstruction to absolute levels.

Acknowledgements

I would like to thank my supervisor Prof. Dr. Ing. Pavel Zemčík, for his help, guidance and excellent ideas. Thank you belong to my consultant in TESCAN, Vojtěch Filip, for providing everything needed for this

work, as well as professional insight and tips. A special thanks go to Jakub Kolář of TESCAN for spending hours on data acquisition. I am very grateful to my family and girlfriend for the constant support and help throughout this endeavour.

References

- [1] P. Eaton and P. West. *Atomic Force Microscopy*. OUP Oxford, 2010. ISBN 9780191576676.
- [2] Yu Zhang, David N. R. Payne, Charlie Kong, Muhammad U. Khan, Tsun H. Fung, Rasmus S. Davidsen, Ole Hansen, Giuseppe Scardera, Malcolm D. Abbott, and Bram Hoex. Advanced characterisation of black silicon surface topography with 3d pfb-sem. In *2019 IEEE 46th Photovoltaic Specialists Conference (PVSC)*, pages 0825–0828, USA, 2019. IEEE.
- [3] Mona Eulitz and Gebhard Reiss. 3d reconstruction of sem images by use of optical photogrammetry software. *Journal of Structural Biology*, 191(2):190–196, 2015. Elsevier Inc., Germany.
- [4] Katsushi Ikeuchi and Berthold K.P. Horn. Numerical shape from shading and occluding boundaries. *Artificial Intelligence*, 17(1):141–184, 1981. Elsevier Inc.
- [5] Joseph I Goldstein, David C Joy, Joseph R Michael, Dale E Newbury, Nicholas W.M Ritchie, and John Henry J Scott. *Scanning Electron Microscopy and X-Ray Microanalysis*. Springer,, Imprint, 4th ed. 2018 edition, 2018. USA.
- [6] Wuyuan Xie, Yunbo Zhang, Charlie C.L. Wang, and Ronald C.-K. Chung. Surface-from-gradients: An approach based on discrete geometry processing. In *2014 IEEE Conference on Computer Vision and Pattern Recognition*, pages 2203–2210, 2014.
- [7] Ludwig Reimer. *Scanning Electron Microscopy*. Springer Berlin Heidelberg, Berlin, Heidelberg, 2nd edition, 1998. ISBN 978-3-642-08372-3.